

Crossover from non-thermal to thermal photoluminescence from metals excited by ultrashort light pulses

Y. Sivan^{1,*}, I. W. Un¹, I. Kalyan¹, K.-Q. Lin², J. M. Lupton², S. Bange²

¹ School of Electrical and Computer Engineering, Ben-Gurion University, Israel

² Institut für Experimentelle und Angewandte Physik, Universität Regensburg, Germany

* To whom correspondence should be addressed; E-mail: sivanyon@bgu.ac.il

February 17, 2023

Abstract

Photoluminescence from metal nanostructures following intense ultrashort illumination is a fundamental aspect of light-matter interactions. Surprisingly, many of its basic characteristics are under ongoing debate. Here, we resolve the majority of these debates by providing the most complete theoretical framework to date that describes this phenomenon, and support it by experimental confirmation. Specifically, we identify aspects of the emission that are characteristic to either non-thermal or thermal emission, in particular, differences in the spectral and electric field-dependence of these two contributions to the emission. Overall, non-thermal emission is characteristic of the early stages of light emission, while the later stages show thermal characteristics. The former dominate only for moderately high illumination intensities for which the electron temperature reached after thermalization is close to room temperature. The theory is then complemented by experimental evidence that demonstrates the novel aspects of our considerations.

1 Introduction

1.1 General background

The emission of light from metals following illumination, known as metal photoluminescence (PL), is a fundamental aspect of light-metal interactions. Surprisingly, this phenomenon is far from being understood, with its main features having been under debate for decades [1]. For example, there is not even agreement on whether the emission is due to electronic Raman scattering (whereby absorption and emission occur with no delay) or due to radiative recombination (for which a delay does

occur), see, e.g., [2]. For the relatively simple scenario of emission under CW illumination, the emission statistics (i.e., bosonic or fermionic or whether it is thermal or non-thermal (sometimes dubbed as “hot” PL) have remained unclear [3, 4], and the interplay between excitation wavelength, resonance position and emission lineshape is still not well understood. It was also not clear whether the emission should be associated with the electron or lattice temperatures, and there were different models describing the scaling of the emission with the electric field amplitude, the value of the quantum yield, etc.

Additional arguments have been put forward specific to PL following illumination by an ultrafast light pulses (to be denoted below as transient PL, tPL). For example, the differences between the emission and scattering spectra were not understood (see, e.g., [5, 6, 7, 8, 9, 10, 11, 12, 13, 4]). Further, in the majority of cases, the emission was associated with two-photon interband transitions (usually referred to as two-photon PL, 2PPL, e.g. [14, 5, 15, 16]), while fewer studies discussed emission occurring within the conduction band (see, e.g, [6, 17, 18, 19, 10, 20]). Furthermore, there is a range of different claims about the electric field dependence of the emission, associated with the *integer* number of photons absorbed at the stage preceding the emission. In particular, there have been reports of linear scaling (see [21, 6, 18]), two-photon absorption (2PA) [22, 15] (or, as said, 2PPL), 3PA [23], multiple power laws (2PA to 4PA [24], 3PA to 5PA [25], 4PA to 6PA [26]) and even up to 8PA [27]. In contrast, some studies explained the emission using a thermal model [2, 17, 28, 29] such that it is thought of as thermal emission from an object with an optically induced transient electron temperature [2, 30, 31]. In particular, in [2] the emission was interpreted via the “Two Temperature Model” (TTM). Such models give rise to *non-integer* power-law scaling, see e.g., [17, 28, 13, 32, 4].

These thermal models for the emission came along with the suggestion to spectrally resolve the emission [2, 17, 28, 25]. Indeed, most earlier experiments measured the total number of emitted photons at all frequencies collected over many pulses. However, the frequency-by-frequency account of the emission in [2] was used to show that the emission cannot originate just from 2PA. In [2, 17, 28], a power-law dependence of the emission on the illuminating field strength was observed experimentally and explained assuming that the emission is purely thermal. In particular, the power exponent of the incident intensity I_{inc} (or equivalently, the irradiance), i.e. the incident field strength squared, with respect to the photon emission rate at a particular emission frequency ω , Γ^{em} was shown to grow linearly with the emission frequency (i.e., $\Gamma^{\text{em}} \sim (I_{\text{inc}})^p$, with $p \sim \hbar\omega$) over a very wide spectral window, for random dense films of both gold and silver nanoparticles NPs and later for sparse gold NP random arrays [28]. Similar results were later obtained in [4, 29] for a gold film and Ga spheres [33]. The model of [17, 28] also explained the growing importance of the blue-side of the emission upon increase of the incident illumination intensity I_{inc} . Not only this study further supported the claim that the emission does not originate from 2PA, but it also served to support the claims that the emission originates from intraband

recombination events [28]. Interestingly, however, in [28] a low intensity measurement revealed a different spectral dependence of the emission on the electric field, namely, a step-like scaling of the square of the local field $|E|^2$ (which is $\sim I_{\text{inc}}$) for the Stokes Emission (SE) and a scaling of $|E|^4 \sim (I_{\text{inc}})^2$ for the anti-Stokes Emission (aSE).

These rather different views of the physical nature of metal PL could be associated with three main reasons. First, the experiments were performed for a wide range of structures and illumination conditions. Second, only very few studies resolved the dynamics of the PL spectrally (e.g., as in [2, 17, 28]) or temporally (e.g., as in [34, 21, ?, 35, 36, 20, 37]) and even fewer resolved both; this prevented obtaining a deep understanding of the PL. Third, there was no comprehensive theoretical basis to explain the experimental data. Indeed, although the dynamics of electrons following an ultrashort pulse was well-understood theoretically and experimentally soon after the emergence of femtosecond lasers (e.g., [38, 39, 40, 41, 42]), this understanding was not employed to resolve any of the above disagreements. Indeed, the first attempt to explain the transient PL from metals using a model that relied on the detailed electron dynamics was made in [43]; it relied on the well-established Boltzmann model for the electron dynamics ([39, 41, 42])¹. The employed approach accounted for the discrete nature of the electron levels (as suitable for 1-2 nm particles [44]). However, it treated the excitation crudely in the sense that its starting point was a maximal deviation from equilibrium due to a pulse with fixed total energy, rather than a proper modelling of the excitation stage. Moreover, while this work treated the $e - e$ transition matrix elements with unusually high accuracy, it treated $e - ph$ interactions phenomenologically, by using the relaxation time approximation, so the total energy of the electron system (hence the intensity of the emission) might not be captured correctly in that work [45, 46].

A somewhat more accurate model was employed in [36] which used state-of-the-art modelling for the $e - e$ and $e - ph$ interactions as well as photon absorption. The PL was, however, computed approximately by assuming that the electron distribution is thermal with an equivalent electron temperature² and using Planck's Law in free space; this is suitable for metal nanostructures illuminated away from any resonance, structures having shallow resonances (which indeed includes the Ag film studied in that work) or when the (localized) plasmon resonance (PR) is in the aSE range, but is less suitable for single particles which have a more pronounced plasmon resonance (a scenario abundant in most other experimental work). Most recently, Riffe and Wilson's similar detailed rigorous analysis of the ultrafast dynamics of electrons following a short pulse was applied to reconstruction of the emission measurements in [2]. In that respect, both these papers did not address directly the disagreements described above.

Thus, the existing work on transient PL from metals does not actually explain if the emission is thermal or non-thermal, and cannot unequivocally determine the

¹However, the photon absorption rate seems to have been vastly overestimated in [43].

²probably as in [41].

scaling of the emission with the electric field. In [37], an attempt to separate the non-thermal and thermal component was made. However, this work also treated the excitation stage crudely, and used rather phenomenological expressions for the electron dynamics.

Below, we rely on recent progress in the understanding of CW PL, and an application of a complete description of the electron non-equilibrium dynamics to answer these open questions, demonstrate the findings in new measurements, and use the model to interpret earlier work.

1.2 Early theory on CW PL

Recently, following the progress made in the calculation of the steady-state electron non-equilibrium in metals under CW illumination [45, 46], Sivan & Dubi studied the corresponding light emission (PL) from the metal [47]. They showed that the emission consists of 2 components. The first is *thermal* (or, black-body, BB) emission, given by Planck's Law, which is proportional to the average energy, namely,

$$\sim \langle \mathcal{E}_{\text{BB}}(\omega, T_e) \rangle = \frac{\hbar\omega}{e^{\frac{\hbar\omega}{k_B T_e}} - 1}, \quad (1)$$

which is enhanced by the Purcell effect (via the multiplication by the local density of photonic states, LDOPS, $\rho_{\text{phot}}(\omega)$); here, ω is the emission frequency, k_B is the Boltzmann constant and T_e is the steady-state electron temperature [45, 46]. The second component is *non-thermal* emission, which, using the approximate analytic solution derived in [46], was found to consist of a series of Planck-*like* terms, namely,

$$\sim \rho_{\text{phot}}(\omega) [A(\omega; \omega_L, T_e) \delta_E + B(\omega; \omega_L, T_e) \delta_E^2 + \dots], \quad (2)$$

where

$$A(\omega; \omega_L, T_e) = 2 \frac{\hbar(\omega - \omega_L)}{e^{\frac{\hbar(\omega - \omega_L)}{k_B T_e}} - 1}, \quad B(\omega; \omega_L, T_e) \sim -2A(\omega; \omega_L, T_e) + \frac{1}{2}A(\omega; 2\omega_L, T_e). \quad (3)$$

Here, ω_L is the frequency of the incoming pump photons and $\delta_E = |\hat{E}(\omega_L)/E_{\text{sat}}|^2$ is the ratio of the local field and the saturation field (see definition in [47]) whose value is ~ 5 GV/m for noble metals. The shifts by ω_L are the signature of the non-thermal (yet, thermal-*like*) nature of the emission originating from one photon absorption events, two-photon absorption (*sequential*, i.e., uncorrelated) events, etc.

For CW, which naturally involves no more than modestly high intensities and electron temperatures, the second term is overwhelmingly dominant over all other terms for most experimentally accessible scenarios (i.e., for realistic temperatures and for frequencies not much higher than ω_L). This makes CW PL a pure non-thermal emission effect (i.e., "hot" PL). It also has a markedly different spectral signature compared to

the thermal emission. Specifically, considering only the electronic contribution to the emission (see Eq. (7) below, obtained by ignoring the LDOPS, or simply normalizing by it), the non-thermal emission alternates between rather flat spectral ranges and those where the emission decays exponentially³; this contrasts with the BB emission which decays exponentially with growing frequency from a maximal value in the deep infrared region, see Fig. 1.

The analysis in [47] enabled the resolution of several long-standing disagreements, e.g., those associated with the statistical nature of the emission, its spectral features, the connection to the electron and phonon temperatures etc.

1.3 Paper outline

In this work, motivated by the analysis of CW metal PL [47], free of simplifying assumptions such as rapid or effective thermalization [2, 17], or neglecting the excitation stage [43, 36] and free of spectral and intensity limitations of an experiment [17, 28], we employ a theoretical framework that is capable of answering the various open questions associated with the nature of transient PL from metals. We begin by providing a heuristic explanation of transient PL, see Section 2. Then, in Section 3, we describe the theoretical model (Section 3.1) and calculate numerically the metal PL by solving the Boltzmann-equation for the transient electron dynamics following illumination by a short pulse of a wide range of intensities (Section 3.2); we then use the extension of the Fermi-golden rule expression for the light emission (derived in [47]) to calculate the PL and identify features that can be associated with either non-thermal or thermal effects, and then separate these contributions into the total transient PL.

The novelty of our approach has two components. First, unlike previous studies in the context of metal PL following illumination by an ultrashort pulse [2, 43, 36], we treat the excitation stage rigorously rather than phenomenologically. Second, inspired by the idea of spectrally resolving the emission introduced in [2, 17, 28] and the analysis of the CW emission (which exposed the different contributions to the emission spectrum), we study the evolution of the emission in time. By correlating the distribution dynamics to the emission dynamics and monitoring the evolution of the spectral structure of the emission, we draw conclusions regarding the relative importance of the thermal and non-thermal components of the emission.

In Section 3.2.2, we then focus on the scaling of the emission with the electric field. We show that at low intensities, the emission is characterized by a power law with a step-like exponent, and that this is a signature of PL based on non-thermal electrons (i.e., “hot” PL). In contrast, at high intensities the power law attains a smooth linear dependence on the emission frequency. As shown already in [17, 28] for the NP clusters and the dense NP films illuminated by relatively high intensities,

³As discussed in [47], this dependence is similar to the step structure seen earlier in the context of ultrafast electron dynamics in, e.g., [48, 41].

this behaviour corresponds to thermal emission. Finally, in Section 3.2.3, we show that cumulative heating (from repeated illumination of one (or more) particles can explain the decreasing slope of the emission intensity with respect to the illumination power (as reported, e.g., in [2, 17]).

In Section 4, we describe new experimental data of tPL from Au rods that demonstrate some of the new aspects of the non-thermal emission stage revealed by our analysis, and discuss the signature of these very aspects in earlier work. In Section 5 we provide a summary of our results and an outlook.

2 Heuristic analysis

Unlike the case of PL under CW illumination [47], an analytic expression for the transient PL is not achievable. Nevertheless, based on the CW solution (Eqs. (1)-(3)), assuming that the electron distribution can be loosely separated into a thermal and non-thermal part (as done frequently in this context [49]), and adopting an “adiabatic” point of view (i.e., treating the electron distributions at each time snapshot as if it was a stationary distribution), we expect the emission to be roughly of the following form⁴

$$\begin{aligned} \Gamma_{\text{tot}}^{\text{em}}(\omega) \sim & \langle \mathcal{E}_{\text{BB}}(\omega; T_e(t)) \rangle + 2\langle \mathcal{E}_{\text{BB}}(\omega - \omega_{L,0}; T_e(t)) \rangle \delta_E(t) \\ & + \langle \mathcal{E}_{\text{BB}}(\omega - 2\omega_{L,0}; T_e(t)) \rangle \delta_E^2(t) + \dots \end{aligned} \quad (4)$$

Here, $\langle \mathcal{E}_{\text{BB}}(\omega, T_e(t)) \rangle$ is, as in Eq. (1), the Planck (BB) term, i.e., it represents the thermal emission, now at a time-varying electron temperature; the next terms represent *non-thermal* (“hot”) emission, even though they involve frequency-shifted Planck (i.e., thermal-*like*) terms; here, $\omega_{L,0}$ is the central frequency of the illuminating laser pulse and $\delta_E = |E(t; \omega_{L,0})/E_{\text{sat}}|^2$ is the ratio of the (now time-varying) envelope of the local field⁵ and the saturation field [47]. As in the CW case, the first non-thermal term is proportional to the square of the local electric field, and the emitted frequency is shifted by one photon-energy quantum. This term matches the expression adopted for the electron-hole occupation number in [2, Eq. (2)]⁶. The third term is due to 2 (uncorrelated events of) photon absorption, etc.

Different from the CW case, here, T_e represents a time-varying effective (/equivalent [41]) electron temperature; there are various ways to determine it⁷, which nevertheless all give qualitatively similar behaviour as well as a value which, upon completion of the thermalization of the electron subsystem, emerges to be the actual electron temperature; *for the purpose of the current heuristic argument*, these approaches are

⁴As seen from Eq. (3), the form adopted here is somewhat simplified and, hence, should not be taken as more than a qualitative description.

⁵i.e., $\mathcal{E} = E(t; \omega_{L,0})e^{-i\omega_{L,0}t} + c.c.$

⁶Note that this term was interpreted implicitly in [2] as having a *thermal* origin; our analysis shows otherwise.

⁷e.g., it can be determined via the total energy of the electron subsystem [41, 50], via energy balance [42], coarse graining the Boltzmann equation [46], a TTM [2] etc.

equivalent. In general, due to the various electron collision mechanisms, the temperature rise is a complicated nonlocal and nonlinear function of the local field. In some simple cases, solving a single temperature equation may suffice, see [51]. In these cases, the electron temperature increases above the ambient temperature T_{amb} with the local electric field simply as

$$T_e = T_{\text{amb}} + \Delta T_e(|E(t; \omega_{L,0})|^2). \quad (5)$$

Several insights can already be obtained from Eqs. (4)-(5). First, the non-thermal contribution clearly decays rapidly. The heuristic form (4) implies this would occur on the timescale of the local electric field; however, clearly, the actual decay rate would be determined by the thermalization rate (i.e., it would be dominated by $e - e$ collisions). In contrast, the BB term persists for longer times, determined in part by $e - ph$ coupling but mostly by the much slower heat transfer to the environment. Thus, one can expect the early stages of the emission to be non-thermal, but the later (post-thermalization) stages to be of a thermal nature.

Second, following the analysis of the CW case [47], we expect the non-thermal emission to be far stronger than the thermal emission; indeed, the latter is generally weak and peaks at the infrared regime. The thermal emission, however, will be gradually stronger with growing illumination intensity, because the overall system will then heat up more and thus make the thermal component stronger and blue-shift it into the visible frequency range. In a standard measurement, the emission is time-integrated, so the statistical nature of the emission will depend on the relative importance of these two contributions.

Third (again, following [47, Fig. 3(b)]), the 2PA term is expected to dominate the aSE above some frequency. Specifically, at $T_e \rightarrow 0$, this frequency is simply $\omega_{L,0}$, and it grows with T_e . Going further, the 3PA term dominates above $2\omega_{L,0}$, and so forth. Correspondingly, the transitions between the spectral regions dominated by m -photon absorption, and $(m + 1)$ -photon absorption smear out for growing T_e .

Lastly, it becomes obvious that for low illumination intensities (for which there is negligible light-induced heating) the dependence of the PL on the electric field is simply polynomial, corresponding to the m -photon absorption terms alluded to above. However, upon significant heating, the polynomial description fails due to the (exponential) dependence of the coefficients $\langle \mathcal{E}(\omega - m\omega_{L,0}; T_e) \rangle$ on the electric field (see Eq. (5)).

Below, we show numerical simulations that support these heuristic expectations. They, however, also show that the heuristic solution (4) captures the dynamics only qualitatively, so (4) will serve only for the purpose of distinguishing the crossover from non-thermal (absorption-induced) emission to thermal (temperature-induced) emission.

3 Theory of transient PL

3.1 Model

Determining the transient PL requires first knowing the transient electron distribution dynamics, $f(\mathcal{E}, t)$. We determine this by solving the time-dependent Boltzmann equation assuming that electron states in the metal are characterized by a continuous energy variable. In [52, 44], it was shown that for NP sizes of ≈ 2 nm the results of this approach are in excellent agreement with the more accurate discretized momentum-space models.

The electron interactions are accounted for using a standard model, not much different from the one used in the original studies of the problem (e.g., [39, 41, 42, 49]), incorporating electron collision mechanisms and emphasizing the rigorous treatment of photon absorption events, see Appendix A⁸. In particular, we account for intraband absorption events as well as interband transitions by accounting for the empirical value used for the imaginary part of the permittivity in Poynting's Theorem⁹. This rigorous treatment of the absorption enables us to study the early stages of the PL dynamics, and hence, to study both the statistical aspects of the emission as well as its dependence on the electric field. This is the main distinction of our work from earlier theoretical studies of the transient emission from metals [43, 36].

As shown in [17, 28, 29], the emission has similar characteristics for different particle geometries; thus, except for its effect on the LDOPS (see below), the nanostructure geometry in our model manifests itself only in the connection of the local field to the incident field. In that respect, we consider only the averaged electric field inside the metal, and rely on the strong electron diffusion [54] to justify the assumption that not only is the temperature uniform in the nanostructure, but also the electron distribution itself.

We verified that even for the most intense illumination level used in this work, the emission is much weaker compared to all the effects accounted for above when calculating the distribution $f(\mathcal{E}, t)$. Thus, the emission can be determined from the distribution via a perturbative calculation (as done previously for CW PL in [47], using time-dependent quantum mechanical perturbation theory (Fermi golden rule)). In particular, in analogy to the steady-state case, the transient PL (from a point in the metal NP) is given by [47]

$$\Gamma^{\text{em}}(\vec{r}, \omega, t) = \frac{\pi\omega V_{\text{NP}}^2}{\epsilon_0} \rho_{\text{phot}}(\vec{r}, \omega) I_{\text{e}}(\omega, t), \quad (6)$$

where V_{NP} is the NP volume, ϵ_0 is the vacuum permittivity, and ρ_{phot} is the LDOPS which is set, for simplicity, to have a Lorentzian-like spectrum centered at ω_{PR} and

⁸Since the electron dynamics were studied systematically in many previous articles [39, 41, 49, 36, 53], we do not show them here explicitly.

⁹Thus, we do not account for 2 simultaneous photon absorption events from the d ('valence') band to the conduction band. In that respect, we are not convinced that earlier claims for the dominance of these transitions were substantiated.

width of $\gamma_{\text{PR}} = \omega_{\text{PR}}/10$. In that sense, we discuss only single-mode emission; it is natural to refer to this mode as the dipolar one, as it is the observable by far-field measurements. This also allows us to suppress the intricate dependence of the LDOPS on the spatial coordinate. Finally, the electronic contribution to the emission is given by

$$I_e(\omega, t) = \int_0^{\mathcal{E}_{\text{max}}} |\vec{\mu}(\mathcal{E}, \mathcal{E} + \hbar\omega)|^2 \rho_J(\mathcal{E}, \mathcal{E} + \hbar\omega, t) d\mathcal{E}, \quad (7)$$

where \mathcal{E}_{max} represents the top of the conduction band, $\vec{\mu}$ is the dipole moment transition matrix element and ρ_J is the population-weighted joint density of pair states, given by

$$\rho_J(\mathcal{E}_f, \mathcal{E}_i, t; \omega_L) = \{f(\mathcal{E}_i, t; |E(\omega_L)|^2) \rho_e(\mathcal{E}_i)\} \{[1 - f(\mathcal{E}_f, t; |E(\omega_L)|^2)] \rho_e(\mathcal{E}_f)\}. \quad (8)$$

Here, $\mathcal{E}_i = \mathcal{E}_f + \hbar\omega_L$ are the initial and final electron energies involved in the absorption of a ω_L photon.

We note that the final state \mathcal{E}_f can, in principle, be either in the conduction band, or in the d ('valence') bands; the corresponding matrix elements for these two processes are comparable¹⁰. In the latter case, the hole occupation is essentially negligible [56, 49], a fact which immediately shows that the contribution of transitions to the lower d ('valence') electron bands is negligible with respect to the intraband PL. This conclusion is in line with the reports of [17, 28, 29] that the (t)PL has similar characteristics for different materials (Au and Ag) and justifies the focusing on the electron distribution in the conduction band only.

Where necessary, in order to mimic the experimental data [2, 17, 28], we integrate the emission over time (for a single excitation pulse). In this case, the total emission is given by

$$\Gamma_{\text{tot}}^{\text{em}}(\omega) \sim \int_0^{1/f_{\text{rep}}} \Gamma^{\text{em}}(\omega, t) dt, \quad (9)$$

where f_{rep} is the pulse repetition rate.

3.2 Numerical results

Following [28], we assume that the Au rod studied in [28] is illuminated by a $\tau_L = 85$ fs-long (Gaussian) laser pulse with a central frequency $\omega_{L,0}$ corresponding to a wavelength of 700 nm and average intensity varying between $I_{\text{av}} = I_0 \tau_L f \sim 0.1 - 30$ kW/cm²¹¹, with $f = 80$ MHz being the pulse repetition rate (i.e., starting at somewhat lower values and going up to somewhat higher values compared to those used in [28]). Notably, the population of high energy electron states never exceeds a few percent even for the highest illumination intensities used.

¹⁰Indeed, converting the value reported in [55] for the expectation value of the momentum operator to the dipole matrix element and ignoring the degeneracy gives $\sim 1.8 \cdot 10^{-29}$ C·m (near the X point of the dispersion relation of the metal), whereas the value obtained from [44] for an energy $\hbar\omega = 1.8$ eV away from the Fermi level is $3.81 \cdot 10^{-29}$ C·m· $\frac{\text{nm}}{L}$ where L is the particle size.

¹¹Hence, the incident intensity is given by $I_{\text{inc}}(t) = I_0 e^{-4 \ln 2 t^2 / \tau_L^2}$, with I_0 being the peak intensity.

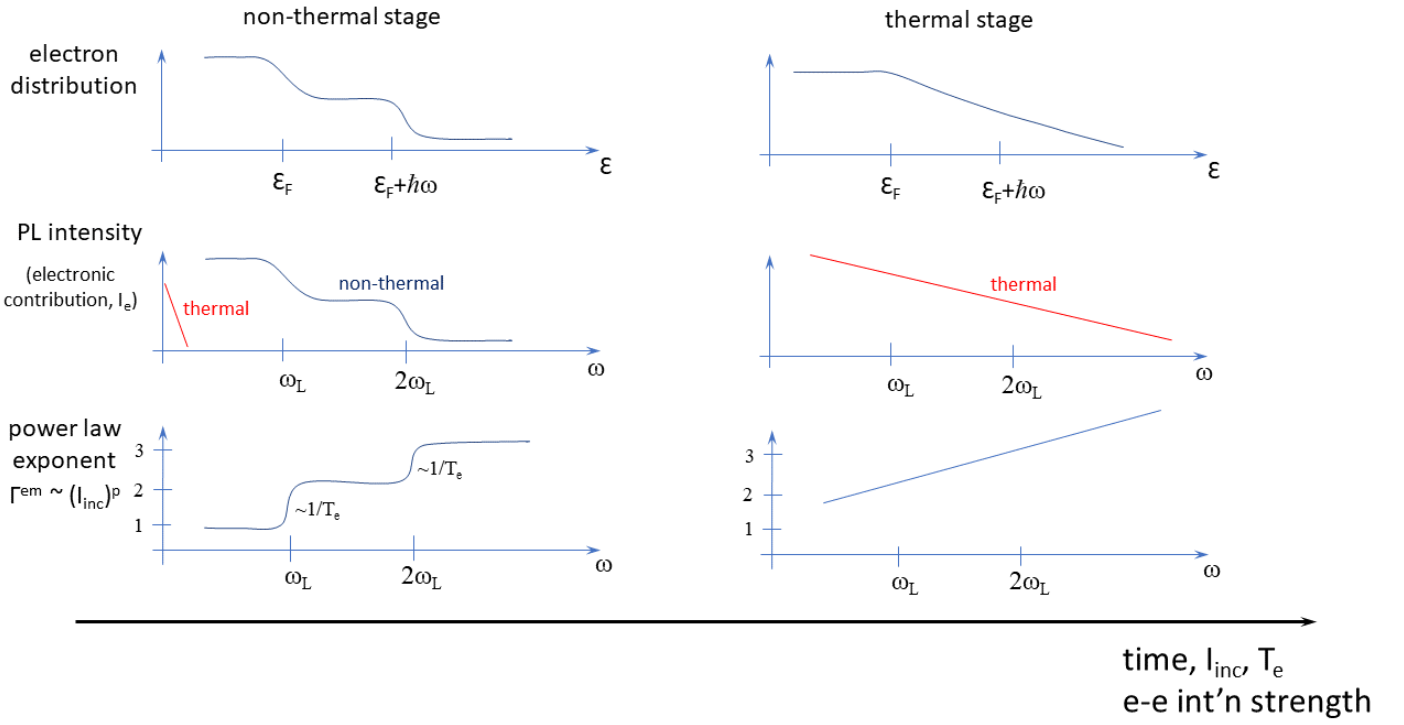


Figure 1: A schematic of electron distribution, the electronic contribution to the emission and the power-law exponent for the non-thermal stage (left) and the thermal stage (right).

3.2.1 The distribution and emission dynamics

We first show the calculated distribution ($f(\mathcal{E}, t)$; Fig. 2(a)) and PL ($\Gamma^{\text{em}}(\omega, t)$; Fig. 2(b)-(c)) for a moderately high energy pulse (0.5 pJ, or $I_{\text{av}} = 0.1 \text{ kW/cm}^2$); for convenience, cross-sections of the electronic contribution to the emission (I_e , Eq. (7)) are shown as well (Fig. 2(d)).

Dynamics. We observe that the emission intensity initially grows together with the illuminating pulse intensity and the high-energy non-thermal electron occupation probability (see Fig. 2(a)-(b)); the emission peaks at a slight delay of a few tens of femtoseconds with respect to the pulse, together with the peak of the high-energy non-thermal electron occupation.

Beyond this stage, the PL intensity decreases with time at a rate that is a non-trivial combination of both $e - e$ and $e - ph$ interactions (see related discussions, e.g., in [38, 49, 20, 57, 36]). Overall, the decay rate is on the order of a few hundred femtoseconds. In that sense, it is slower compared to the pulse duration¹² and the decay of the high energy electron occupancy (determined by $e - e$ collisions), but commensurate with the decay rate of the effective electron temperature (determined by $e - ph$ collisions) as deduced from the total energy in the electron subsystem (see Fig. 2(a)).

¹²This discrepancy illustrates the inaccuracy of the heuristic analysis of Section 2.

A more careful look at these data sets shows that the emission of high-frequency photons decays faster than the emission of lower-frequency photons (Fig. 2(b)); this observation matches the experimental observation in [20, Fig. 1]. This is also in line with Fermi's liquid theory (FLT) [58], which predicts that the electron collision rate is faster the further away the energy is from the Fermi energy, i.e., $\tau_{e-e}^{-1} \sim [(\pi k_B T_e)^2 + (\mathcal{E} - \mathcal{E}_F)^2]$. Indeed, as shown as early as in [59], the occupation of higher-energy electrons decays faster than that of lower-energy electrons, thus reducing the probability of high-frequency photon emission. Being a characteristic of the transition from a non-thermal to a thermal distribution, this observation further supports the interpretation of the peak, i.e. early emission as non-thermal light emission.

As discussed in [36, 53], the dynamics are affected only in a modest quantitative manner by somewhat different $e - e$ interaction strengths (compare [36, Figs. 4(b)-(c)]). For the purpose studied here, stronger $e - e$ interactions would make the thermal emission component relatively stronger compared to the non-thermal part. Similarly, there are only modest quantitative changes for longer illumination pulses, amounting to a smearing of the electron distribution and PL dynamics.

However, the dynamics are modified more significantly when the illumination intensity increases. Under such conditions, the thermalization occurs more rapidly [59, 49, 20, 36] and we observe that the decay rate of the emission becomes slower with increasing illumination intensity, even reaching several thousands of femtoseconds for the higher illumination levels (see Fig. 3); this rate is commensurate with the decrease in dynamics of the effective electron temperature (Fig. 3(a)-(b)). As a result, the contribution to the emission from the early (non-thermal) stages of the dynamics is not as important for strong illumination compared to moderate illumination.

Because of all this, at the later stages of the emission and for higher excitation intensities, the emission should be thought of as dominantly thermal light, in agreement with the interpretation in [2]¹³ and [17, 28, 29]. Simply put, the reason for the stronger thermal characteristic at higher intensities is that under these conditions, T_e is higher, so the thermal component is correspondingly more significant.

One should also note that the thermal component of the emission persists until the arrival of the next pulse in the pulse train, i.e., far longer than the sub-picosecond extent of the non-thermal emission. This is particularly significant for the aSE (e.g., the green curve in Fig. 2(b)) and for high intensities (Fig. 3(b)), for which the peak of the emission (the non-thermal component) is only a few orders of magnitude higher than the late emission (i.e. the thermal component); thus, when the emission is integrated in time, the orders-of-magnitude longer extent of the thermal emission may convey a higher relative importance of thermal emission compared to a time-resolved data acquisition. In that respect, the repetition rate may affect the conclusion about the nature of the emission if judged via the time-integrated spectrum.

Emission spectra. As shown in see Fig. 2(c)-(d), the spectrum of the emitted light in the initial stages of the dynamics exhibits the step-like structure observed in

¹³obtained by studying emission from longer pulses (0.45 and 2 ps).

the CW case [47] over which the LDOPS is superimposed; in particular, the emission spectrum is determined by the LDOPS, but its blue side is quenched by the electronic contribution, I_e . This structure, however, gets gradually smeared into the monotonically-decreasing spectra characteristic of thermal emission. Fig. 4(a) shows that the (time-integrated) emission is eventually dominated by the PR lineshape. Notably, this figure also shows that the blue (aSE) side of the emission spectrum broadens with growing illumination intensity, as predicted and observed in [17, 28]. The reason for this is that the aSE is connected to the thermal part of the electron distribution and of the emission (see discussion in [19, 60, 3, 47]), which naturally grows with the illumination intensity¹⁴.

An additional aspect of the transient emission, which has been under debate, is the dynamics of the spectral lineshape. Unlike the claim in [43], we observe in Fig. 2(c), Fig. 3(c) and Fig. 4(a) that the peak of the emission spectrum does not vary in time. However, the red side of the spectrum decays more slowly than the blue side. This behaviour can, again, be traced to the overall decrease in the occupation of high-energy electron states, resulting in an overall red-shift of the integrated spectra. Notably, for systems with a flat resonance (such as films), this effect manifests itself as a continuous red-shift of the spectrum, see the measurements in [20].

3.2.2 Quantifying the dependence on the electric field

The time-integrated emission spectra shown in Fig. 4(a) enables the extraction of the dependence of the tPL on the electric field strength. In particular, we linearly fit a double-logarithmic representation of the emission $\Gamma_{\text{tot}}^{\text{em}}$ as a function of irradiance I_{inc} for each frequency in the emission spectrum, i.e., we determine the spectrum of the power-law coefficient p in $\Gamma_{\text{tot}}^{\text{em}} \sim (I_{\text{inc}})^p$. For this purpose, typically only a narrow range of irradiances is used such that p constitutes an effective coefficient of nonlinearity *local* in both emitted photon energy and illuminating irradiance.

In Fig. 4(b) we show the results of the application of the power law extraction algorithm of [17, 28] on the numerical data shown in Section 3.2. For *moderately high* illumination intensities, one can see a rather clear step structure. Specifically, we obtain $p = 1$ for the SE and $p = 2$ for the (low frequency) aSE; at emission frequencies higher than $2\hbar\omega_{\text{L},0}$, we observe an additional step of $p = 3$, which has not been reported before. This observation is in line with the predictions of the heuristic model (Section 2) and hence, is a clear signature of the dominance of the tPL by recombination of non-thermal electrons. Remarkably, this step-like behaviour also matches the experimental observations of tPL in [28, Fig. 3(b)] for low illumination intensity from a single Au nanorod; for the aSE, a $p = 2$ exponent was also observed in [2, Fig. 2B]¹⁵. Notably, this power law is attained even in the absence of interband

¹⁴This behaviour was referred to as a spectral blue-shift [17, 28, 43]; indeed, the moments of the emitted spectra blue-shift.

¹⁵Our model also matches the observation in [21] of a $p = 1$ exponent for the integrated spectrum, which is naturally dominated by the SE.

transitions, so the popular attribution of the PL nonlinearity to simultaneous two-photon interband transitions, dating back as early as [14, 5], does not seem to be of a general nature. Instead, one should understand the result as an effective nonlinearity averaged over multiple sequential electron excitation pathways, as pointed out by Knittel *et al.* [61].

Spectrally narrow transitions between these regimes of constant nonlinearity are found at frequencies near integer multiples of the excitation laser frequency. The shape of these transitions is a reflection of the electron distribution existing before the arrival of the laser pulse and can be used to determine the average lattice temperature. With increasing temperature, the transitions distinctly shift towards lower photon energies, as detailed in Appendix B. As the illumination intensity increases, the staircase-like pattern in the power-law spectrum gradually evolves into a straight line. This is a clear signature of thermal emission, as it was shown in [17] that for thermal electron distributions

$$\log \left[(\mathcal{E}_{\text{BB}}(|E|^2)) / (\mathcal{E}_{\text{BB}}(|E_0|^2)) \right] \sim p(\hbar\omega) \log(|E|^2 / |E_0|^2),$$

with $p(\hbar\omega) = \hbar\omega / (a k_B T_0)$ based on the assumption that the illumination intensity-dependence of the electron temperature follows $(T/T_0)^a = |E|^2 / |E_0|^2$ as expected for an electron gas. Here, E_0 and T_0 are some reference field and temperature and a being an order unity dimensionless number¹⁶. Remarkably, this transition happens for low frequencies (SE) at relatively low intensities and for high frequencies (aSE) at higher intensities. This agrees with the above heuristic interpretation, namely, that the thermal contribution becomes stronger and shifts from the infrared into the visible spectral range as the illumination intensity grows.

We note, however, that the power-law exponent is shown on a limited spectral range for growing illumination intensities. The reason for this is that the emission at such frequencies would not only depend on the exact population at low electron energies in the conduction band, but also on the population of the various d ('valence') bands which are not accounted for in the current study. Moreover, the high frequency emission will be limited by the band edge (vacuum level). Therefore, we are careful not to provide a prediction of the power law exponent for such high frequency - high intensity regime.

3.2.3 The role of cumulative (steady-state) heating and permittivity changes

In all our calculations, we neglected the small transient changes to the permittivity following each pulse absorption event [49]. However, even though the absorbed heat is mostly transferred to the environment by the arrival of the next pulse, a small fraction of it may increase the temperature of the NP and environment slightly. Thus, it is clear that the temperature of the system will gradually grow due to accumulation

¹⁶This is indeed the high temperature limit of Eq. (10) for $a = 2$.

of this residual absorbed energy after a sufficiently large number of pulses [62, 63]. This effect becomes stronger in case of heating from adjacent illuminated NPs [62, 63, 64]. Such cumulative heating (of both electron and phonon temperatures) by several hundreds of degrees is expected to cause changes to the (steady-state) metal permittivity [65, 66, 67] and, hence, to reduce the local field strength [68, 69, 70], such that the steady-state temperature rise will become sublinear with respect to the irradiance. Eventually, the heating will cause surface melting and volume changes, particle reshaping and ultimately sample damage [71, 72].

In order to determine this long-term steady-state temperature rise via numerical simulations, one needs to know the details of the nanostructure geometry, the pulse repetition rate, the outer thermal boundary conditions, etc. (see, e.g., [63]). Instead, for simplicity, we estimate the cumulative heating in the specific case of [28] as follows: We assume that the sample reaches the temperature threshold for damage/sintering (estimated to be $T_{\text{amb}} \sim 550$ K [67]) due to cumulative heating for average illumination intensities of 12.5 kW/cm 2 (i.e., slightly exceeding the highest used in [28]). Fig. 4(c) shows that this causes a slight increase of the emission intensity in comparison to the case of $T_{\text{amb}} = 300$ K. Indeed, initially the aSE is higher, and as the system thermalizes, the SE intensity also increases slightly.

However, for resonant illumination, this slight increase in emission intensity is overwhelmed by a stronger effect - the imaginary part of the metal permittivity increases [65, 66, 67]¹⁷, and consequently, the quality factor of the plasmon resonance drops and the local field decreases [74, 68, 69, 70]. As a result, the emission intensity decreases across the entire spectrum (again, see Fig. 4(c)). As the illumination is shifted away from resonance, this effect becomes gradually weaker (not shown).

In this respect, our results explain the experimental observations of a decreasing power exponent of the aSE in the high-power range in [2, Fig. 2B] and in [17]¹⁸. Our explanation refines the proposal in [2] that σ_{abs} grows for high electron temperatures. The latter claim was shown in [68, 69, 70] to hold only for off-resonance frequencies.

4 Experiments

The linear power-law spectrum $p \sim \hbar\omega$ discussed in Section 3.2.2 has been observed by several groups for metal NPs excited by ultrashort laser pulses [17, 18, 33, 4] and can be understood reasonably well by the analysis of a thermalized electron gas [17] as discussed above. On the other hand, the transition between the low-irradiance, staircase-like and the high-irradiance, linear power-law spectrum has so far only been reported once [28] and the physical nature of the underlying nonlinearity was not

¹⁷An exception is the regime of wavelengths shorter than ~ 500 nm, which is dominated by interband transitions [73, 67].

¹⁸Note that a similar effect occurs due to the temperature dependence of the electron heat capacity [75, 17]; however, such an effect is associated with the ultrafast electron dynamics, rather than the steady-state heating that is discussed in the current section.

fully understood.

The model presented so far attributes the low-irradiance nonlinearity to the effective number of photon excitation necessary to excite the electronic states contributing to the joint density of states ρ_J (Eq. (8)), even when the transitions happen sequentially within the (same) conduction band (see Appendix B). Two critical predictions can be derived that so far lack experimental confirmation: first, moderate-irradiance power-law spectra acquire a staircase-like structure with integer values for the power-law coefficient, even beyond the value of $p = 2$ demonstrated in [28]. Second, transitions between the spectral regions of integer power-law coefficients m and $m + 1$ follow the position of the integer multiple of the laser frequency $m\omega_L$. To confirm these predictions, we measured the PL spectra of 86 nm-long gold nanorods terminated by cetyltrimethylammonium bromide (CTAB) with a diameter of 22 nm and a volume of $3.3 \pm 0.6 \cdot 10^{-23} \text{ m}^3$.

The nanoparticles were dropcasted from a sufficiently diluted aqueous solution onto a standard microscope cover slip after thorough substrate cleaning by ultrasonication with an alkaline cleaning solution (Hellma Hellmanex, 3% concentration) and 30 min of UV-ozone treatment to remove residual fluorescence from surface contaminations. Excitation by ultrafast laser pulses (Coherent Chameleon Ultra) through a 500 mm-focal-length lens and an oil-immersion, high-numerical-aperture microscope objective (Olympus 60X TIRF, 1.49 numerical aperture) effectively illuminated surface regions 20 μm in diameter, allowing for control of the illumination irradiance. Detection of the emitted luminescence through the same objective used a 680 nm shortpass filter (Semrock) to block the scattered laser radiation. The spectra were dispersed using a reflective grating with 300 grooves per mm in a spectrograph of 300 mm focal length (Princeton Instruments) and detected by a cooled charge coupled device camera (Princeton Instruments Pixis 100B). Integration times between 2 s and 30 s per spectrum were used for the data discussed here.

Figure 5(a) shows the luminescence spectra for illumination by 160 fs-long laser pulses at $\hbar\omega_L = 1.170 \text{ eV}$, below their localized plasmon resonance at 1.62 eV (see supporting information for the extinction spectrum). Apart from the filter cutoff at 1.91 eV, the spectra cover the whole visible range. The narrow spectral feature is assigned to surface second-harmonic generation (SHG).

Emission spectra were collected for a set of irradiances between 1.2 kW/cm^2 and 2.2 kW/cm^2 , while ensuring the absence of photodegradation by comparing results for upwards and downwards sweeps of the laser power. The power-law coefficient p was extracted as described before by fitting a linear relationship to a double-logarithmic representation of luminescence signal strength and excitation power. At the lowest emitted photon energies, the resulting power-law spectrum in the lower panel of Fig. 5(a) shows a power-law coefficient of 2 similar to the results discussed in [28]. At close to twice the incident photon energy, the distinct, smooth transition between $p = 2$ and $p = 3$ expected from the theory presented above is indeed found, except for the spectral position of the SHG, for which p drops to 2 as expected. The staircase-like

power-law spectrum can be modeled reasonably well even without including electron-electron or electron-phonon scattering, with the shape of the transition region being determined by the average phonon temperature, which is estimated at approximately 500 K. Figure 5(b) shows the same sample region illuminated by 144 fs-long laser pulses at $\hbar\omega_L = 1.374$ eV, closer to the plasmon resonance, for a similar range of irradiation levels between 1.8 kW/cm^2 and 3.1 kW/cm^2 . Although approximately one order of magnitude brighter, the luminescence spectra are comparable to the situation before, with the spectral position of the SHG signal shifted towards higher photon energies. The power-law spectra extracted again show a staircase-like transition between $p = 2$ at low photon energies and $p = 3$ at higher photon energies, with the transition region shifted to twice the incident photon energy. This confirms that the observed step-like power-law spectrum is directly linked to the occurrence of step edges in the electron distribution at integer multiples of the laser photon energy above the Fermi level. This signature of the non-thermal nature of the emission at moderately high illumination level is found to be in line with the estimates of the maximal electron temperature reached (see [76] or Appendix C), namely, 345 K for the data in Fig. 5(a) and 500 K for the data in Fig. 5(b), as well as an analysis of the effect of temperature on the shape of the step edges. The lower panels of Fig. 5 plot the shape of the power-law spectra expected for an electron temperature of 500 K, calculated in the absence of electron-electron or electron-phonon scattering (see Appendix B). Indeed, for these low temperatures, the thermal emission still occurs at wavelengths far into the mid infrared.

Higher-order power-law coefficients can only be reached by longer-wavelength laser excitation to avoid the photoionization threshold. Fig. 5(c) shows data extracted from [25] for gold nanorods of 320 nm length excited by 130 fs laser pulses at $\hbar\omega_L = 0.61$ eV. The power-law spectrum can be understood reasonably well by our model - the obvious deviations indicate the onset of the thermal emission regime and the increased relevance of electron-electron and electron-phonon scattering over the relevant timescale of the luminescence.

5 Summary and outlook

In this work, we have reconciled the different views on the importance of the thermal and non-thermal components in PL from metals following illumination by a short laser pulse. Specifically, we find that in the moderately high and ultrashort illumination limit, the emission is dominantly non-thermal at the early stages; the behaviour in this regime is thus similar to what happens for emission under CW illumination [47], for which the illumination intensity is relatively weak and the non-equilibrium component in the electron distribution persists permanently. The dependence on the electric field strength in this regime is given by a “staircase” of integer powers (see Fig. 1), smoothed by the electron temperature. This dependence is rooted in the absorption process. Under these conditions, analysis that relies only on the second term in Eq. (4)

(e.g., [2]) is valid. However, the emission at the later stages and/or for more intense (e.g., [29]) pulses gradually attains more and more thermal characteristics. Indeed, under such conditions, the transient effective temperature in the Planck term grows significantly so that the thermal emission shifts from the IR to the visible range and becomes stronger. In this case, one should interpret the emission using only the first (Planck) term in Eq. (4) (e.g. [30, 29]) and reference to the emission as thermal light emitted by an object with a time-varying temperature (see [2, 17, 28, 30, 31]) is valid as well¹⁹.

The model we used to explain the PL and to match the experimental data considers single-photon intraband absorption. However, multiphoton interband absorption events may also affect the PL dynamics and the spectrum, especially at high intensities and for high frequency emission. In fact, most earlier studies associated the PL with such interband transitions (see e.g., [14, 15, 5, 16]), even when photons of energies lower than the interband threshold were used; in this case, the emission must indeed originate from *simultaneous* 2PA events. Unfortunately, it is very hard to model this effect properly, because the 2PA cross-section is not well characterized and because of the complexity of the d ('valence') bands. In contrast, our model accounts for *uncorrelated* photon absorption events within the conduction band, an effect which yields a similar higher-order dependence on the electric field strength associated with the emission spectrum as described above. Notably, uncorrelated multiphoton absorption events are far more likely compared with simultaneous ones; for the same reason, radiative recombination is more likely to be responsible for one-photon emission compared with electronic Raman transitions (see discussion in [2, 1]).

Further studies are required to resolve these issues, as well as to decipher the complex polarization dependence of NPs of more complicated structure under very high excitation intensities [78]. For these purposes, time-resolved PL spectroscopy (as employed, e.g., in [34, 21, ?, 20, 36, 37]) will be of great value. Our work also allows for quantitative interpretation of transient thermometry studies based on the aSE [79], and will be crucial for further studies of other emission processes, such as cathodoluminescence and electroluminescence.

Acknowledgements. I.W., I.K. and Y.S. were partially funded by a Lower-Saxony - Israel collaboration grant no. 76251-99-7/20 (ZN 3637) as well as an Israel Science Foundation (ISF) grant (340/2020).

A Model description

The photoluminescence is determined perturbatively from the non-equilibrium electron distribution, which in turn, is determined by solving the Boltzmann equation. It

¹⁹This is similar to the observations regarding the PL from a semiconductor (except, possibly for the exceptionally high illumination intensities) [77], which are correctly referred to as "PL by thermalized systems" [30, 31].

incorporates three generic terms [45, 46]. First, $e - e$ interactions are described by the (standard) 4-particle interaction integral (see e.g., [39, 48, 40, 41, 80, 36]), i.e., without the relaxation time approximation; for simplicity, we assume momentum-independent hard-sphere interactions, but verified that the results described below do not change qualitatively if we change the strength of the $e - e$ interactions²⁰. Second, $e - ph$ interactions are computed as in [39, 45]. Third, the key novelty in our formulation concerns the photon-electron interaction, which is based on the formulation described in [39, 42, 45]; this form enables us to monitor the electron distribution in the early stages of the dynamics.

We emphasize that our model accounts for two (or more) photon absorption from consecutive (and hence, uncorrelated) intraband transition events (but not for the much less likely simultaneous absorption event of two or more photons).

Unlike the CW case [45, 46], there is no analytical solution for f , which now depends in an implicit way on the details of the illumination. We also avoid defining the electron temperature, although we do refer to an effective (or equivalent [41]) value for it that emerges to be the actual electron temperature in the later stages of the dynamics (see, e.g., [39, 41]). Also note that in this approach there is no assumption on the scaling of the heat capacity with temperature, as this quantity emerges naturally from the rigorous electronic calculations. Furthermore, heat transfer to the environment was neglected, as it occurs on a longer timescale than relevant for the PL and affects the PL only marginally.

B The shape of power-law spectra at moderate irradiances

For moderate excitation pulse energies, the shape of the power-law exponent spectrum is determined to a large degree by the electron distribution present before the arrival of the laser pulse. Fig. 6 shows the electron distribution for laser excitation at 1.375 eV together with typical transitions contributing to the PL emission. Before accounting for electron-electron or electron-phonon scattering, photoexcitation of the electron distribution results in characteristic “shelves” of the density of states (estimated as constant, for simplicity), each being associated with an effective integer nonlinearity. These shelves are connected by Fermi-like transitions. For a chosen emitted photon energy, the characteristic interaction orders for the occupied and the unoccupied states add up to the associated total effective nonlinearity, or power-law coefficient. To determine the power-law exponent spectra, the emission is calculated in the range of 80% to 125% of a given reference excitation pulse energy and fitted linearly on a double-logarithmic scale. The results are plotted against the emitted photon energy in Fig. 7. An increase of the initial electron temperature softens the transition re-

²⁰This can be thought of as a way to mimic $e - e$ interactions more accurately, such as the momentum-dependent Thomas-Fermi formulation, etc.

gions between individual plateaus in the staircase-like power-law spectrum. For the lower excitation pulse energies, increased temperatures induce pronounced shifts of the transition region towards higher photon energies. This effect is caused by the increased occupation in the high-energy tails of the Fermi distributions, cf. Fig. 6. This shift can be used as an estimate of the effect of heat accumulation caused by the pulsed excitation at high repetition rates, as the initial electron temperature is equal to the phonon temperature.

C Characteristics of the gold nanorod sample

Gold nanorods terminated by cetyltrimethylammonium bromide (CTAB) were synthesized as described in [81]. Based on a characterization by scanning electron microscopy, the rod length was 86 ± 6 nm, and the diameter 22 ± 2 nm. The extinction spectrum and an SEM image is shown in Fig. 8(a). Samples were fabricated on thoroughly cleaned microscope cover slips by dropcasting. Fig. 8(b) shows the absorption cross-section $\sigma_{\text{abs}}(\omega)$ of the rods, along with the spectra of two pulses used to generate the data in Fig. 5 (a)-(b).

Following [76], it can be shown that the maximal electron temperature can be approximated by

$$\max(T_e) \approx \sqrt{T_{\text{amb}}^2 + 2Q/\gamma}, \quad (10)$$

where $Q = \sigma_{\text{abs}}(\omega)I_0\tau_L/V$ is the power absorbed by the nanorod following illumination by a single pulse (see Section 3.2), V the rod volume, and $\gamma = 67 \text{ J/m}^3\text{K}^2$ the proportionality constant between the electron heat capacity and the electron temperature (i.e., $C_e = \gamma T_e$ [75]).

As this relation neglects the non-thermal stage of the dynamics, as well as energy transfer from the electrons to the phonons, it provides no more than a reasonable estimate to the actual heat dynamics. Nevertheless, for the current purposes, it enables an estimate of the wavelength of maximal thermal emission via Wien's displacement law, $\lambda_{\text{peak}} = c/\nu_{\text{max}}$ where $\nu_{\text{max}} = 5.879 \cdot 10^{10} \max(T_e)$.

References

- [1] G. Baffou. Anti-Stokes thermometry in nanoplasmonics. *ACS Nano*, 15:5785–5792, 2021.
- [2] J. Huang, W. Wang, C. J. Murphy, and D. G. Cahill. Resonant secondary light emission from plasmonic Au nanostructures at high electron temperatures created by pulsed-laser excitation. *Proc. Nat. Acad. Sci. U.S.A.*, 111:906–911, 2014.

- [3] A. Carattino, M. Calderola, and M. Orrit. Gold nanoparticles as absolute nano-thermometers. *Nano Lett.*, 18:874–880, 2018.
- [4] Y.-Y. Cai, E. Sung, R. Zhang, L. J. Tauzin, J. G. Liu, B. Ostovar, Y. Zhang, W.-S. Chang, P. Nordlander, and S. Link. Anti-Stokes emission from hot carriers in gold nanorods. *Nano Lett.*, 19:1067–1073, 2019.
- [5] G. T. Boyd, Z. H. Yu, and Y. R. Shen. Photoinduced luminescence from the noble metals and its enhancement on roughened surfaces. *Phys. Rev. B*, 33:7923, 1986.
- [6] M. Beversluis, A. Bouhelier, and L. Novotny. Continuum generation from single gold nanostructures through near-field mediated intraband transitions. *Phys. Rev. B*, 68:115433, 2003.
- [7] A. Bouhelier, R. Bachelot, G. Lerondel, S. Kostcheev, P. Royer, and G. P. Wiederrecht. Surface plasmon characteristics of tunable photoluminescence in single gold nanorods. *Phys. Rev. Lett.*, 95:267405, 2005.
- [8] M. Yorulmaz, S. Khatua, P. Zijlstra, A. Gaiduk, and M. Orrit. Luminescence quantum yield of single gold nanorods. *Nano Lett.*, 12:4385–4391, 2012.
- [9] A. Tcherniak, S. Dominguez-Medina, W.-S. Chang, P. Swanglap, L. S. Slaughter, C. F. Landes, and S. Link. One-photon plasmon luminescence and its application to correlation spectroscopy as a probe for rotational and translational dynamics of gold nanorods. *J. Phys. Chem. C*, 115:15938–15949, 2011.
- [10] J. Mertens, M.-E. Kleemann, R. Chikkaraddy, P. Narang, and J. J. Baumberg. How light is emitted by plasmonic metals. *Nano Lett.*, 17:2568–2574, 2017.
- [11] H. Hu, H. Duan, J. K. W. Yang, and Z. X. Shen. Plasmon-modulated photoluminescence of individual gold nanostructures. *ACS Nano*, 6:10147–10155, 2012.
- [12] T. Yin, Z. Dong, L. Jiang, L. Zhang, H. Hu, C.-W. Qiu, J. K. W. Yang, and Z. X. Shen. Anomalous shift behaviors in the photoluminescence of dolmen-like plasmonic nanostructures. *ACS Photonics*, 3:979–984, 2016.
- [13] Y.-Y. Cai, J. G. Liu, L. J. Tauzin, D. Huang, E. Sung, H. Zhang, A. Joplin, W.-S. Chang, P. Nordlander, and S. Link. Photoluminescence of gold nanorods: Purcell effect enhanced emission from hot carriers. *ACS Nano*, 12:976–985, 2018.
- [14] A. Mooradian. Photoluminescence of metals. *Phys. Rev. Lett.*, 22:185, 1969.
- [15] P. Ghenuche, S. Cherukulappurath, T. H. Taminiau, N. F. van Hulst, and R. Quidant. Spectroscopic mode mapping of resonant plasmon nanoantennas. *Phys. Rev. Lett.*, 101:116805, 2008.

- [16] S. Grossmann, D. Friedrich, M. Karolak, R. Kullock, E. Krauss, M. Emmerling, G. Sangiovanni, and B. Hecht. Nonclassical optical properties of mesoscopic gold. *Phys. Rev. Lett.*, 122:246802, 2019.
- [17] T. Haug, P. Klemm, S. Bange, and J. M. Lupton. Hot-electron intraband luminescence from single hot spots in noble-metal nanoparticle films. *Phys. Rev. Lett.*, 115:067403, 2015.
- [18] K.-Q. Lin, J. Yi, S. Hu, J.-J. Sun, J.-T. Zheng, X. Wang, and B. Ren. Intraband hot-electron photoluminescence from single silver nanorods. *ACS Photonics*, 3:1248–1255, 2016.
- [19] J. T. Hugall and J. J. Baumberg. Demonstrating photoluminescence from Au is electronic inelastic light scattering of a plasmonic metal: The origin of SERS backgrounds. *Nano Lett.*, 15:2600–2604, 2015.
- [20] T. Suemoto, K. Yamanaka, and N. Sugimoto. Observation of femtosecond infrared luminescence in gold. *Phys. Rev. B*, 100:125405, 2019.
- [21] E. Dulkeith, T. Niedereichholz, T. A. Klar, J. Feldmann, G. von Plessen, D. I. Gittins, K. S. Mayya, and F. Caruso. Plasmon emission in photoexcited gold nanoparticles. *Phys. Rev. B*, 70:205424, 2004.
- [22] K. Imura, T. Nagahara, and H. Okamoto. Near-field two-photon-induced photoluminescence from single gold nanorods and imaging of plasmon modes. *J. Phys. Chem. B*, 109:13214–13220, 2005.
- [23] Richard A. Farrer, Francis L. Butterfield, Vincent W. Chen, and John T. Fourkas. Highly efficient multiphoton-absorption-induced luminescence from gold nanoparticles. *Nano Lett.*, 5:1139–1142, 2005.
- [24] P. Mülschlegel, H.-J. Eisler, O. J. F. Martin, B. Hecht, and D. W. Pohl. Resonant optical antennas. *Science*, 5:308, 2005.
- [25] V. Knittel, M. P. Fischer, M. Vennekel, T. Rybka, A. Leitenstorfer, and D. Brida. Dispersion of the nonlinear susceptibility in gold nanoantennas. *Phys. Rev. B*, 96:125428, 2017.
- [26] Q. Ai, L. Gui, D. Paone, B. Metzger, M. Mayer, K. Weber, A. Fery, and H. Giessen. Ultranarrow second-harmonic resonances in hybrid plasmon-fiber cavities. *Nano Lett.*, 18:5576–5582, 2018.
- [27] R. Méjard, A. Verdy, M. Petit, A. Bouhelier, B. Cluzel, and O. Demichel. Energy-resolved hot-carrier relaxation dynamics in monocrystalline plasmonic nanoantennas. *ACS Photonics*, 3:1482–1488, 2016.

- [28] L. Roloff, P. Klemm, I. Gronwald, R. Huber, J. M. Lupton, and S. Bange. Light emission from gold nanoparticles under ultrafast near-infrared excitation: Thermal radiation, inelastic light scattering, or multiphoton luminescence? *Nano Lett.*, 17:7914–7919, 2017.
- [29] K. Malchow and A. Bouhelier. Photon bunching of the nonlinear photoluminescence emitted by plasmonics metals. *Journal of the Optical Society of America B*, 38:576, 2021.
- [30] J.-J. Greffet, P. Bouchon, G. Brucoli, and F. Marquier. Light emission by nonequilibrium bodies: Local kirchhoff law. *Phys. Rev. X*, 8:021008, 2018.
- [31] L. Wojszvzyk, H. Monin, and J.-J. Greffet. Light emission by a thermalized ensemble of emitters coupled to a resonant structure. *Adv. Optical Mater.*, 7:1801697, 2019.
- [32] J. Chen, A. Krasavin, P. Ginzburg, A. V. Zayats, T. Pullerits, and K. J. Karki. Evidence of high-order nonlinearities in supercontinuum white-light generation from a gold nanofilm. *ACS Photonics*, 5:1927–1932, 2018.
- [33] J. Xiang, J. Chen, S. Jiang, M. Panmai, P. Li, Y. Xu, Q. Dai, S. Tie, and S. Lan. Liquid gallium nanospheres emitting white light. *Las. Phot. Rev.*, 13:1800214, 2019.
- [34] Y.-N. Hwang, D. H. Jeong, H.J. Shin, D. Kim, S. C. Jeoung, S. H. Han, J.-S. Lee, and G. Cho. Femtosecond emission studies on gold nanoparticles. *J. Phys. Chem. B*, 106:7581–7584, 2002.
- [35] S. Ono. Thermalization in simple metals: Role of electron-phonon and phonon-phonon scattering. *Phys. Rev. B*, 97:054310, 2018.
- [36] S. Ono and T. Suemoto. Ultrafast photoluminescence in metals: Theory and its application to silver. *Phys. Rev. B*, 102:024308, 2020.
- [37] T. Suemoto, K. Yamanaka, N. Sugimoto, Y. Kobayashi, T. Otsu, S. Tani, and T. Koyama. Relaxation dynamics of hot electrons in the transition metals Au, Ag, Cu, Pt, Pd, and Ni studied by ultrafast luminescence spectroscopy. *J. Appl. Phys.*, 130:025101, 2021.
- [38] R. H. M. Groeneveld, R. Sprik, and A. Lagendijk. Femtosecond spectroscopy of electron-electron and electron-phonon energy relaxation in Ag and Au. *Phys. Rev. B*, 51:11433–11445, 1995.
- [39] N. Del Fatti, C. Voisin, M. Achermann, S. Tzortzakis, D. Christofilos, and F. Valleé. Nonequilibrium electron dynamics in noble metals. *Phys. Rev. B*, 61:16956–16966, 2000.

- [40] P. Grua, J. P. Morreeuw, H. Bercegol, G. Jonusauskas, and F. Vallée. Electron kinetics and emission for metal nanoparticles exposed to intense laser pulses. *Phys. Rev. B*, 68:035424, 2003.
- [41] L. D. Pietanza, G. Colonna, S. Longo, and M. Capitelli. Non-equilibrium electron and phonon dynamics in metals under femtosecond laser pulses. *Eur. Phys. J. D*, 45:369–389, 2007.
- [42] J. R. M. Saavedra, A. Asenjo-García, and F. Javier García de Abajo. Hot-electron dynamics and thermalization in small metallic nanoparticles. *ACS Photonics*, 3:1637–1646, 2016.
- [43] J. G. Liu, H. Zhang, S. Link, and P. Nordlander. Relaxation of plasmon-induced hot carriers. *ACS Photonics*, 5:2584–2595, 2018.
- [44] J. B. Khurgin and U. Levy. Generating hot carriers in plasmonic nanoparticles: When quantization does matter? *ACS Photonics*, 7:547–553, 2020.
- [45] Y. Dubi and Y. Sivan. “hot electrons” in metallic nanostructures - non-thermal carriers or heating? *Light: Sci. Appl.*, 8:89, 2019.
- [46] Y. Sivan, I. W. Un, and Y. Dubi. Assistance of plasmonic nanostructures to photocatalysis - just a regular heat source. *Faraday Discuss.*, 214:215–233, 2019.
- [47] Y. Sivan and Y. Dubi. Theory of “hot” photoluminescence from Drude metals. *ACS Nano*, 15:8724–8732, 2021.
- [48] B. Rethfeld, A. Kaiser, M. Vicanek, and G. Simon. Ultrafast dynamics of nonequilibrium electrons in metals under femtosecond laser irradiation. *Phys. Rev. B*, 65:214303, 2002.
- [49] T. Stoll, P. Maioli, A. Crut, N. Del Fatti, and F. Vallée. Advances in femto-nano-optics: ultrafast nonlinearity of metal nanoparticles. *Eur. Phys. J. B*, 87:260, 2014.
- [50] I. W. Un, S. Sarkar, and Y. Sivan. An electronic-based model of the optical non-linearity of low density drude materials. <https://arxiv.org/pdf/2210.08504.pdf>, 2022.
- [51] G. Baffou and R. Quidant. Thermo-plasmonics: Using metallic nanostructures as nano-sources of heat. *Laser Photon. Rev.*, 7:171–187, 2013.
- [52] L. Genzel, T. P. Martin, and U. Kreibig. Dielectric function and plasma resonances of small metal particles. *Z. Phys., B, Condens. matter.*, 21(4):339–346, Dec 1975.

[53] D. M. Riffe and R. B. Wilson. Excitation and relaxation of non-thermal electron energy distributions in metals with application to gold. <https://arxiv.org/abs/2210.09422>.

[54] A. Block, M. Liebel, R. Yu, M. Spector, Y. Sivan, J. García de Abajo, and N. F. van Hulst. Tracking ultrafast hot-electron diffusion in space and time by ultrafast thermomodulation microscopy. *Science Advances*, 5:eaav8965, 2019.

[55] A. Marini, M. Conforti, G. Della Valle, H. W. Lee, Tr. X. Tran, W. Chang, M. A. Schmidt, S. Longhi, P. St. J. Russell, and F. Biancalana. Ultrafast nonlinear dynamics of surface plasmon polaritons in gold nanowires due to the intrinsic nonlinearity of metals. *New. J. Phys.*, 15:013033, 2013.

[56] R. Rosei. Temperature modulation of the optical transitions involving the fermi surface in Ag: Theory. *Phys. Rev. B*, 10:474–483, 1974.

[57] R. B. Wilson and S. Coh. Parametric dependence of hot electron relaxation timescales on electron-electron and electron-phonon interaction strengths. *Commun. Phys*, 3:035424, 2020.

[58] P. Coleman. *Introduction to many body physics*. Cambridge University Press, 2015.

[59] W. S. Fann, R. Storz, H. W. K. Tom, and J. Bokor. Electron thermalization in gold. *Phys. Rev. B*, 46:13592, 1992.

[60] X. Xie and D. G. Cahill. Thermometry of plasmonic nanostructures by anti-Stokes electronic Raman scattering. *Appl. Phys. Lett.*, 109:183104, 2016.

[61] V. Knittel, M. P. Fischer, T. de Roo, S. Mecking, A. Leitenstorfer, and D. Brida. Dispersion of the nonlinear susceptibility in gold nanoantennas. *ACS Nano*, 9:894–900, 2015.

[62] Y. Sivan, I. W. Un, and Y. Dubi. Thermal effects - an alternative mechanism for plasmonic-assisted photo-catalysis. *Chem. Sci.*, 11:5017–5027, 2020.

[63] I. W. Un and Y. Sivan. Parametric study of temperature distribution in plasmon-assisted photocatalysis. *Nanoscale*, 12:17821–17832, 2020.

[64] G. Baffou, I. Bordacchini, A. Baldi, and R. Quidant. Simple experimental procedures to discern photothermal processes in plasmon-driven chemistry. *Light: Sci. Appl.*, 9:108, 2020.

[65] H. Reddy, U. Guler, A. V. Kildishev, A. Boltasseva, and V. M. Shalaev. Temperature-dependent optical properties of gold thin films. *Optical Materials Express*, 6:2776–2802, 2016.

[66] H. Reddy, U. Guler, K. Chaudhuri, A. Dutta, A. V. Kildishev, V. M. Shalaev, and A. Boltasseva. Temperature-dependent optical properties of single crystalline and polycrystalline silver thin films. *ACS Photonics*, 4:1083–1091, 2017.

[67] P.-T. Shen, Y. Sivan, C.-W. Lin, H.-L. Liu, C.-W. Chang, and S.-W. Chu. Temperature- and -roughness dependent permittivity of annealed/unannealed gold films. *Opt. Exp.*, 24:19254, 2016.

[68] Y. Sivan and S.-W. Chu. Nonlinear plasmonics at high temperatures. *Nanophotonics*, 6:317–328, 2017.

[69] I. Gurwich and Y. Sivan. A metal nanosphere under intense continuous wave illumination - a unique case of non-perturbative nonlinear nanophotonics. *Phys. Rev. E*, 96:012212, 2017.

[70] I. W. Un and Y. Sivan. The thermo-optic nonlinearity of single metal nanoparticles under intense continuous-wave illumination. *Phys. Rev. Mater.*, 4:105201, 2020.

[71] K. Setoura, Y. Okada, and S. Hashimoto. CW-laser-induced morphological changes of a single gold nanoparticle on glass: observation of surface evaporation. *Phys. Chem. Chem. Phys.*, 14:26938, 2014.

[72] L. Hou, M. Yorulmaz, N. R. Verhart, and M. Orrit. Explosive formation and dynamics of vapor nanobubbles around a continuously heated gold nanosphere. *New J. Phys.*, 17:013050, 2015.

[73] T. Stoll, P. Maioli, A. Crut, S. Rodal-Cedeira, I. Pastoriza-Santos, F. Vallée, and N. Del Fatti. Time-resolved investigations of the cooling dynamics of metal nanoparticles: Impact of environment. *J. Phys. Chem. C*, 119:12757–12764, 2015.

[74] S.-W. Chu, T.-Y. Su, R. Oketani, Y.-T. Huang, H.-Y. Wu, Y. Yonemaru, M. Yamamoto, H. Lee, G.-Y. Zhuo, M.-Y. Lee, S. Kawata, and K. Fujita. Measurement of a saturated emission of optical radiation from gold nanoparticles: Application to an ultrahigh resolution microscope. *Phys. Rev. Lett.*, 112:017402, 2014.

[75] N. W. Ashcroft and N. D. Mermin. *Solid state physics*. Brooks/Cole, 1976.

[76] Christophe Voisin, Natalia Del Fatti, Dimitris Christofilos, and Fabrice Vallée. Ultrafast electron dynamics and optical nonlinearities in metal nanoparticles. *The Journal of Physical Chemistry B*, 105(12):2264–2280, 2001.

[77] S. Sarkar, I. W. Un, Y. Sivan, and Y. Dubi. Theory of non-equilibrium “hot” carriers in direct band-gap semiconductors under continuous illumination. *New J. Phys.*, 24(5):053008, may 2022.

- [78] Q. Ai, H. Zhang, J. Wang, and H. Giessen. Multiphoton Photoluminescence in Hybrid Plasmon-Fiber Cavities with Au and Au@Pd Nanobipyramids: Two-Photon vs. Four-Photon Processes and Rapid Quenching. *ACS Photonics*, 8:2088, 2021.
- [79] T. Jollans, M. Calderola, Y. Sivan, and M. Orrit. Effective electron temperature measurement using time-resolved anti-Stokes photoluminescence. *J. Phys. Chem. A*, 124:6968–6976, 2020.
- [80] B.Y. Mueller and B. Rethfeld. Relaxation dynamics in laser excited metals under nonequilibrium conditions. *Phys. Rev. B*, 87:035139, 2013.
- [81] K.-Q. Lin, J. Yi, S. Hu, B.-J. Liu, J.-Y. Liu, X. Wang, and B. Ren. Size effect on sers of gold nanorods demonstrated via single nanoparticle spectroscopy. *The Journal of Physical Chemistry C*, 120:20806–20813, 2016.

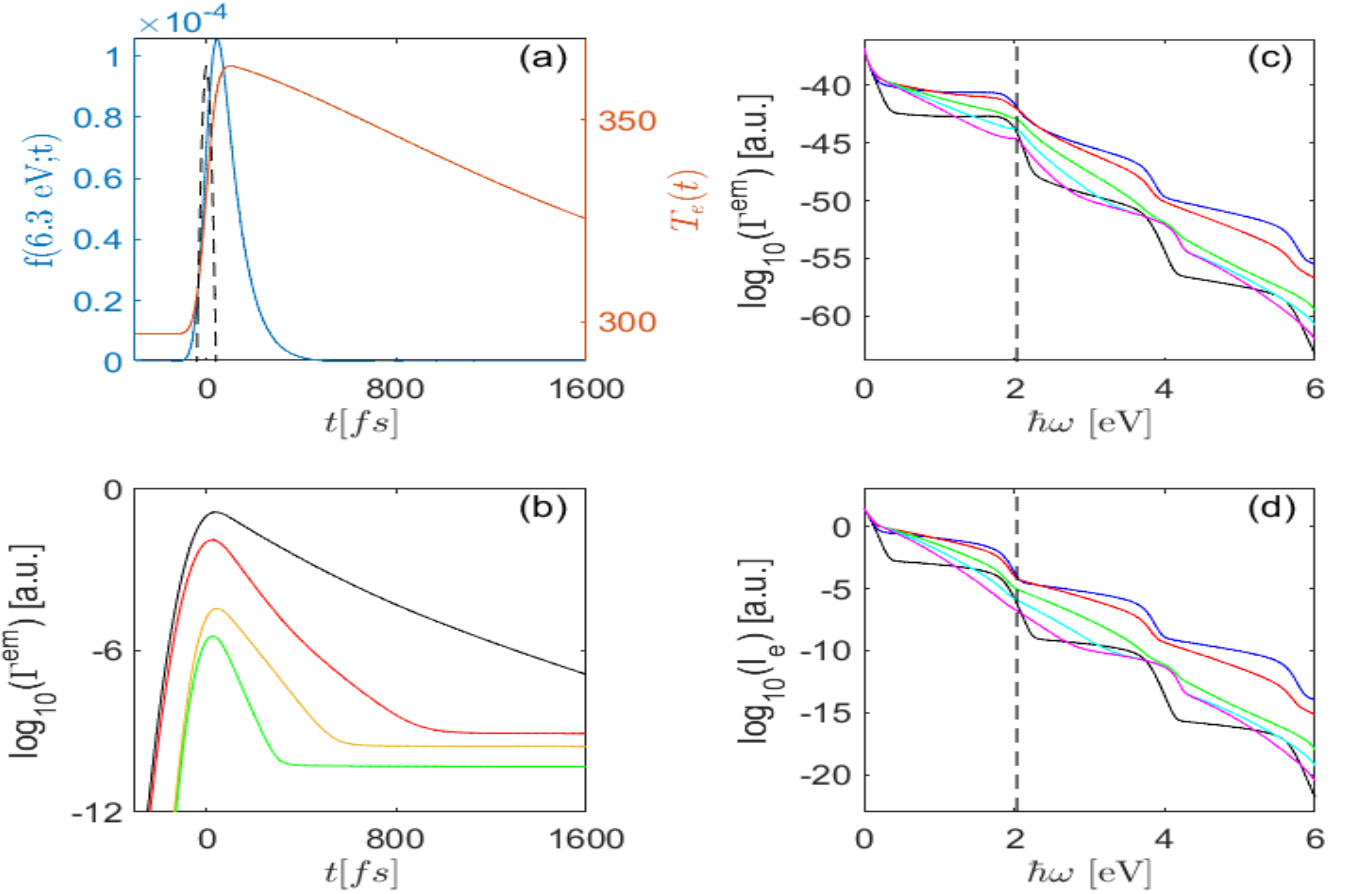


Figure 2: Metal PL following illumination by a 0.5 pJ ($I_{\text{av}} = 0.1 \text{ kW/cm}^2$), 85 fs-long pulse centered at $\hbar\omega_{\text{L},0} = 1.77 \text{ eV}$. (a) Dynamics of the electric field (dashed black line), electron distribution (at the high energy of 6.3 eV; blue) and effective electron temperature (orange). (b) $\log_{10}[\Gamma^{\text{em}}(\hbar\omega = 1.05, 1.77, 2.36, 3.28 \text{ eV}; t)]$ shown by black, red, orange and green solid lines; the emission at the higher frequencies is naturally weaker, but also decays faster due to FLT. (c) PL spectra at different times, $\log_{10}[\Gamma^{\text{em}}(\omega; t = -100, 0, 100, 200, 300, 400 \text{ fs})]$, shown in black, blue, red, green, cyan and magenta solid lines. (d) Same for $I_e(\omega, t)$. The vertical dashed black line in the plots shows the position of the plasmon resonance (PR) at $\hbar\omega_{\text{PR}} = 1.15\omega_{\text{L},0} \cong 2 \text{ eV}$.

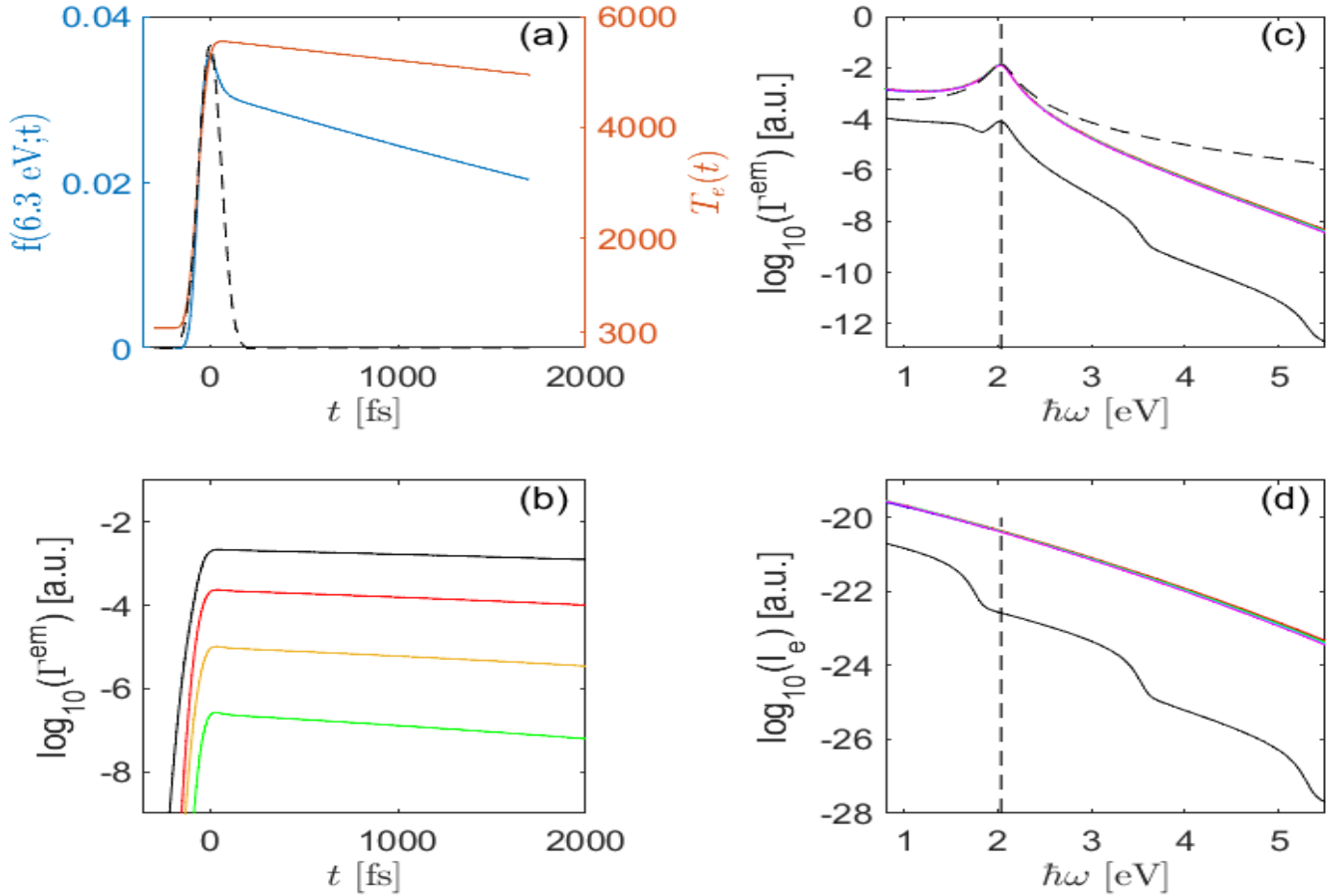


Figure 3: Same as in Fig. 2 for an incident pulse energy of 175 pJ ($I_{av} = 30 \text{ kW/cm}^2$). The almost immediate emergence of thermal characteristics in the electronic distribution is apparent.

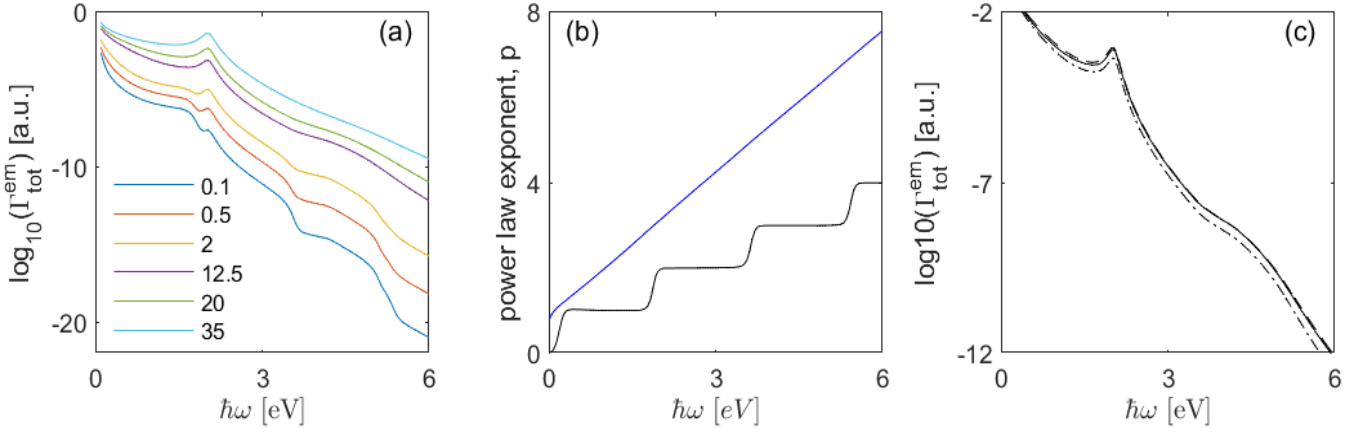


Figure 4: (a) Time-integrated PL spectra as a function of emission frequency for different illumination intensities. The legend corresponds to the values of the average incident illumination intensity I_{av} in kW/cm^2 . (b) Power-law exponent for low excitation intensity (circa 1 pJ; black) and high intensity (circa 50 pJ; blue) extracted with the algorithm described in [17, 28] from the numerical data (see Section 3.2). (c) Time-integrated emission spectra for an illuminating pulse energy of 62.5 pJ ($I_{\text{av}} = 12.5 \text{ kW/cm}^2$). The spectra accounting for 300 K and 550 K background temperatures are shown by the solid and dashed lines, respectively, and the dynamics accounting also for the reduced quality factor (due to the increased imaginary part of the permittivity) is shown by the dash-dotted lines.

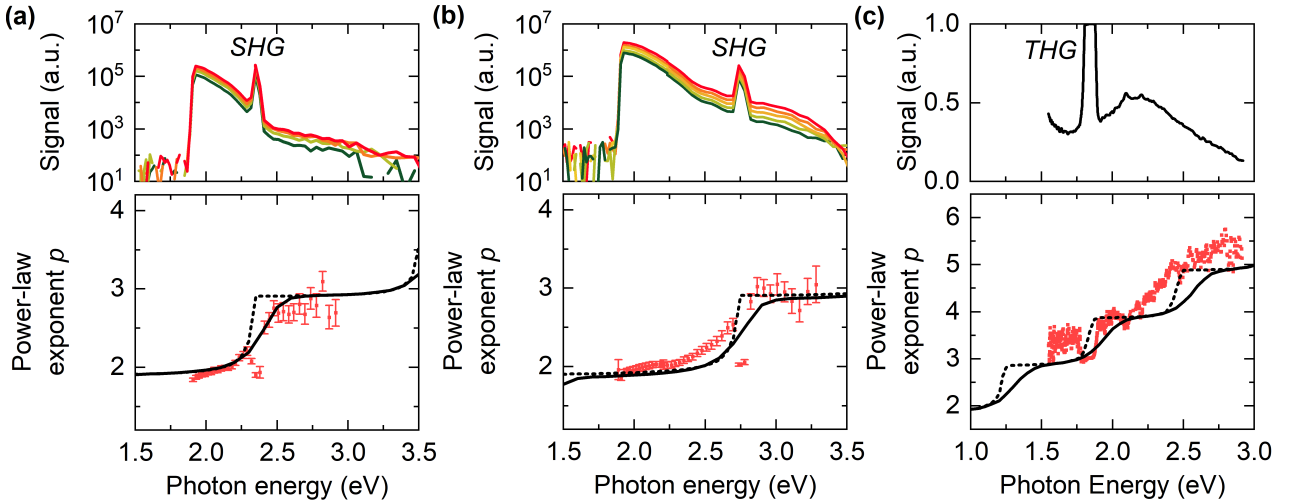


Figure 5: Emission spectra (top panels) and power-law spectra (bottom panels) for 86 nm-long gold nanorods excited at (a) 1.170 eV, 160 fs, 1.2 – 2.2 kW/cm^2 average intensity and (b) at 1.375 eV, 144 fs, 1.8 – 3.1 kW/cm^2 . Panel (c) shows data taken from [25] for 320 nm-long gold nanorods excited with 130-fs pulses at a photon energy of 0.61 eV. Solid (dashed) black lines show the power-law exponents in the emission expected from a simplified model neglecting $e - e$ and $e - ph$ scattering for an initial temperature of 500 K (5 K). Coherent nonlinear optical scattering signals corresponding to second-harmonic generation (SHG) and third-harmonic generation (THG) are marked in panels (a)-(c).

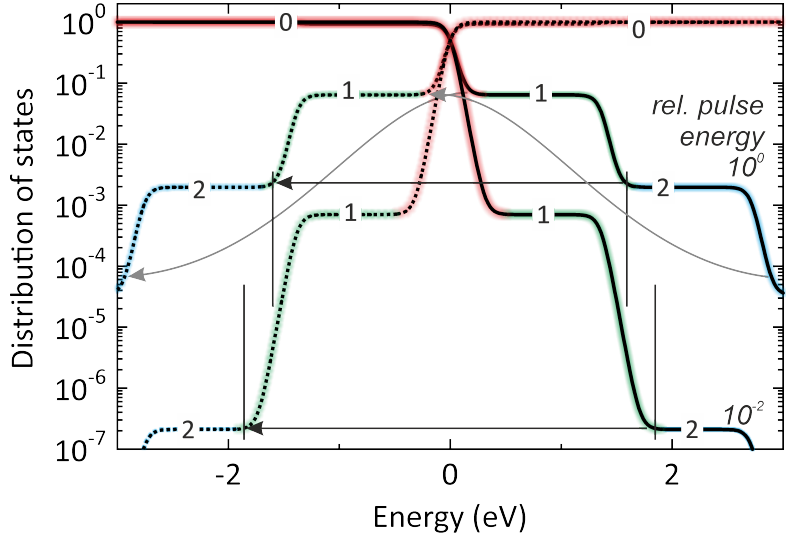


Figure 6: Schematic electron energy distribution relative to the Fermi edge after excitation by 1.375 eV photons. Occupied states (solid lines) and unoccupied states (dashed lines) are shown for two levels of the excitation pulse energy. The effective nonlinear interaction order between photoexcitation and electron occupation associated with each step-like structure is marked by integer digits and red (0), green (1) and blue (2) colors. The maximum photon energy for emission associated with each effective nonlinearity depends on the excitation strength, as marked by the curved black arrows. Note that the other transitions contribute equally (gray arrows).

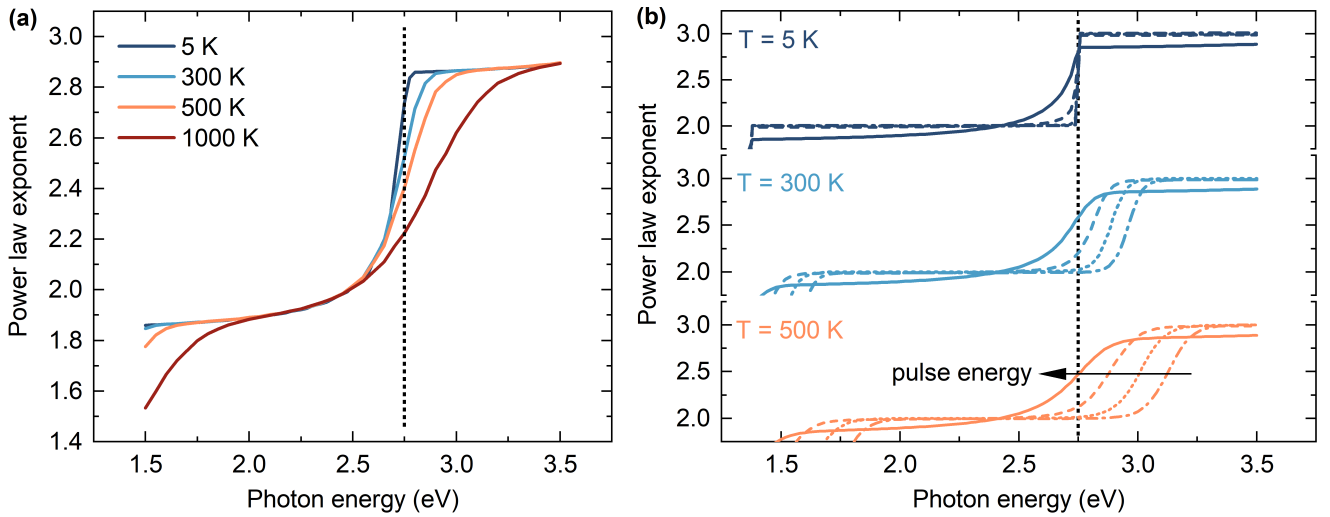


Figure 7: Variation of the shape of step edges in the power-law exponents of the emission spectrum for excitation at 1.375 eV photon energy. Panel (a) shows the effect of the initial electron temperature before taking electron-electron and electron-phonon scattering into account, in the regime of moderately high laser pulse energies. Panel (b) shows the effect of changing the excitation pulse energy at three different temperatures. The dotted line marks a photon energy of 2.750 eV, twice the energy of the excitation photons. Pulse energies reduced by factors of 10^{-1} , 10^{-2} , and 10^{-3} are shown as dashed, dotted, and dash-dotted lines.

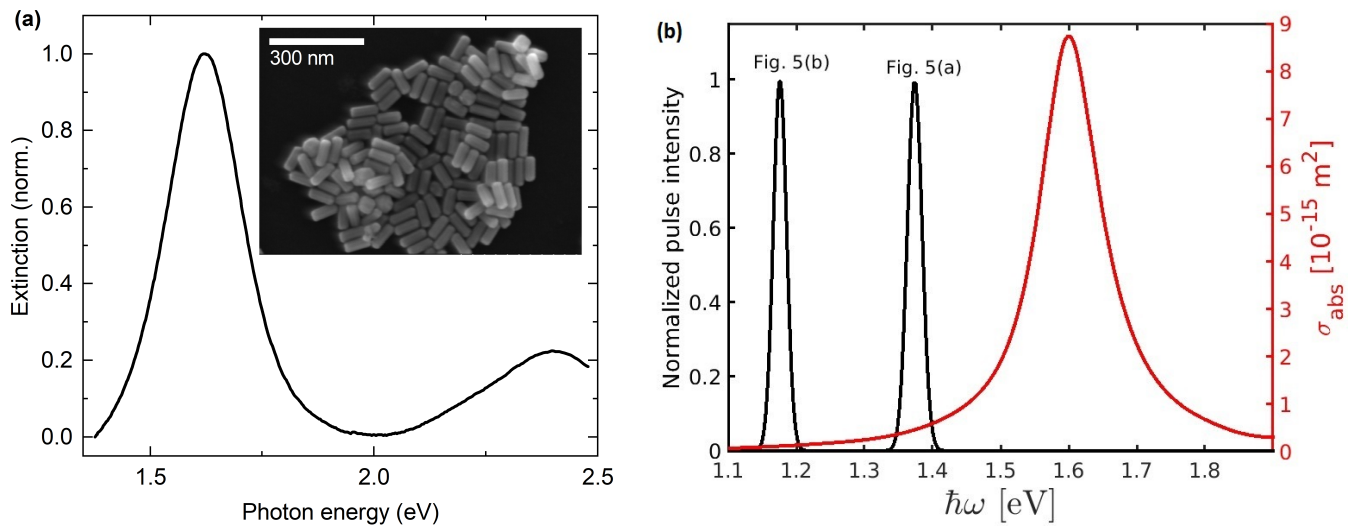


Figure 8: Panel (a) shows the normalized extinction spectrum for the CTAB-terminated gold nanorods. The inset shows a scanning electron micrograph of the particles. Panel (b) shows the calculated absorption cross-section as a function of wavelength, together with the normalized laser spectra for the wavelengths used in Fig. 5 (a)-(b).